separations

MDPI

Article

Preparation, Characterization, and Mechanism of SMS Titanium–Manganese Nanocomposite for Antimony Removal from Water

Yannan Lv [1,2,†], Wenqing Wen [1,2,†], Shenrui Han [1,2], Kaixin Li [2], Ziyu Fu [2], Fansong Mu [1,3,*] and Meng Luo [1,2,4,*]

[1] Yazhou Bay Innovation Institute, Hainan Tropical Ocean University, Sanya 572025, China; lyn13610665848@163.com (Y.L.); wwq17786981136@163.com (W.W.); shenrui_han@163.com (S.H.)
[2] College of Ecology and Environment, Hainan Tropical Ocean University, Sanya 572022, China; lkx200312@outlook.com (K.L.); ink_0522@163.com (Z.F.)
[3] College of Science, Hainan Tropical Ocean University, Sanya 572022, China
[4] Hainan Key Laboratory for Coastal Marine Eco-Environment and Carbon Sink, Sanya 572022, China
* Correspondence: fansong8867@nefu.edu.cn (F.M.); wslm_5555@hntou.edu.cn (M.L.)
† These authors contributed equally to this work.

Abstract: This study investigates the synthesis of SMS-Ti-Mn (SMS-Ti-Mn stands for spent mushroom substrate activated carbon-Ti-Mn) nanocomposites and their application in removing the heavy metal antimony from water. In the process of antimony mining and smelting, the concentration of antimony in the waste residue can still reach as high as 80.5 mg/L. In addition, the soil in the electronic waste dismantling area is severely contaminated with antimony. In short, antimony enters the environment in various ways from mining, smelting, and manufacturing to the final waste process and continuously migrates in different environmental media, increasing the environmental exposure risk of antimony pollution. Single-factor experiments and response surface methodology were employed to determine the optimal conditions, including the adsorption time, pH, and solid–liquid ratio. Material characterization was performed to understand the role of nano-metals, and adsorption kinetics were analyzed using the quasi-first-order kinetic model. The research results revealed that the optimal conditions for antimony removal were an adsorption time of 40 min, a pH of 4, and a solid–liquid ratio of 2:1 (mg/mL). Under these conditions, the nanocomposites showed an adsorption capacity of 10.502 mg/g, which was 5.8 times higher than that of iron coagulants, 11 times higher than that of manganese-modified activated carbon, and 1.7 times higher than that of iron–manganese sludge adsorbents. Characterization revealed enhanced functional groups (carbonyl, Ti=O, Mn=O), contributing to improved adsorption. Kinetic analysis indicated physical adsorption as the dominant mechanism, and the regression model accurately predicted the adsorption capacity. SMS-Ti-Mn nanocomposites offer a promising strategy for treating antimony-contaminated water, with strong potential for practical applications in water treatment. They can decompose naturally after use, reduce secondary pollution, and promote ecological balance. Secondly, agricultural waste treated with heavy metal removal can be used as a fertilizer and soil amendment to improve soil quality and promote sustainable agricultural development.

Keywords: SMS-Ti-Mn nanocomposites; adsorption kinetics; nano-metals; activated carbon; heavy metal removal; water treatment technology

check for updates

Academic Editor: Gavino Sanna

Received: 26 December 2024
Revised: 26 January 2025
Accepted: 27 January 2025
Published: 6 February 2025

Citation: Lv, Y.; Wen, W.; Han, S.; Li, K.; Fu, Z.; Mu, F.; Luo, M. Preparation, Characterization, and Mechanism of SMS Titanium–Manganese Nanocomposite for Antimony Removal from Water. *Separations* **2025**, *12*, 38. https://doi.org/10.3390/separations12020038

Copyright: © 2025 by the authors. Licensee MDPI, Basel, Switzerland. This article is an open access article distributed under the terms and conditions of the Creative Commons Attribution (CC BY) license (https://creativecommons.org/licenses/by/4.0/).

1. Introduction

Research has shown that antimony pollution in water environments is mainly related to factors such as the distribution of antimony minerals, mining development, and mineral demand [1]. Antimony is often found in mining areas and surrounding water bodies. The development and processing of mines are considered important sources of antimony and lead pollution in the environment. In the investigation of antimony pollution, it was found that the antimony concentration in water samples within the investigation range was 4.5–29.4 mg/L, with an average of 10.0 mg/L [2]. In the process of antimony mining and smelting, the concentration of antimony in the waste residue can still reach as high as 80.5 mg/L. The continuous wear of brake pads during braking will release antimony particles into the atmosphere, which will then deposit in nearby soil and water [3]. In addition, the soil in the electronic waste dismantling area is severely contaminated with antimony [4]. In short, antimony enters the environment in various ways from mining, smelting, and manufacturing to the final waste process and continuously migrates in different environmental media, increasing the environmental exposure risk of antimony pollution.

Nanomaterials have demonstrated significant potential in water treatment due to their unique physical and chemical properties [5]. Nano-metal materials offer several advantages, such as large specific surface areas and strong reactivity, but also have limitations, including susceptibility to oxidation, small sizes, easy agglomeration, and difficulty in separation from pollutants [6]. To enhance the activity and stability of nano-metal materials, researchers have attached them to larger carriers [7], improving their shortcomings while taking full advantage of nanoscale features [8], while recent research has focused on using activated carbon as a carrier for nano-metals. As nano-titanium and nano-manganese are both inexpensive and readily available [9], many scholars have used activated carbon combined with nano-metals to prepare new adsorption materials, which not only have the advantages of activated carbon but also improve adsorption performance and enhance mechanical strength, changing the surface. In terms of formaldehyde removal, the catalytic process of activated carbon loaded with nano-metals becomes very rapid [10], and the efficiency of heavy metal removal is also enhanced [11–13]. For instance, when removing thallium from water, it has been observed that the removal percentage increased to 80.4% after loading nano-metals [14]. Similarly, the removal efficiency of nutrient elements like nitrogen and phosphorus using activated carbon nanocomposites loaded with nano-metals increased to seven or eight times that before loading [15]. In nature, antimony often forms jamesonite with lead, which releases antimony and its compounds during mining and processing. Burning antimony-containing minerals or coal may also release antimony. When antimony pollution occurs, it is often accompanied by lead pollution, so in addition to antimony pollution, lead pollution must also be removed. This study prepared SMS-Ti-Mn nanocomposites by combining nano-titanium oxide (TiO_2) and nano-manganese oxide (MnO_2) with modified activated carbon, and took into account the effect of lead removal during material preparation, making the material more advantageous in removing antimony ores from wastewater.

Through a systematic investigation of the preparation process, characterization, and adsorption properties of SMS-Ti-Mn nanocomposites, we developed an efficient and economical SMS-Ti-Mn nanocomposite material for removing the heavy metal antimony from water. We aimed to elucidate the removal mechanism of antimony and optimize the adsorption process of the material. By utilizing agricultural waste mushroom bran as a raw material, combined with technologies such as high-temperature carbonization, acid activation, and nanomaterial loading, using analytical techniques such as SEM, FTIR, and XRD, and combining single-factor experiments with response surface methodology to optimize the experiment design, we determined the best preparation conditions for SMS-

Ti-Mn nanocomposites and developed an adsorption kinetics model, thereby providing a scientific foundation for applying these materials in practical water treatment scenarios. The results offer a new strategy for heavy metal water treatment and provide essential theoretical and practical guidance for nanocomposite design and application. The use of agricultural waste as a raw material to prepare adsorbents can reduce environmental pollution, reduce the ecological burden brought by incineration and landfill, and help realize the recycling of resources. Agricultural waste treated for heavy metal removal can be used as a fertilizer and soil amendment to improve soil quality and promote sustainable agricultural development.

2. Materials and Methods

2.1. Reagent Materials

Discarded mushroom residue was collected from the tea tree mushroom planting base in Dahe Village, Chishui Town, Guangchang County, Fuzhou City, Jiangxi Province. Its main raw materials included cedar sawdust and cottonseed.

An antimony standard solution and lead standard solution were purchased from the National Nonferrous Metals and Electronic Materials Analysis and Testing Center, while nano-manganese oxide and nano-titanium oxide were purchased from Zhongse New Materials and MCC New Materials, respectively. The conventional chemical reagents used in the experiment were all analytically pure.

2.2. Preparation of SMS-Based Activated Carbon

Excess mycelium was removed, and the fungus chaff was rinsed, dried at 60 °C, pulverized, and sieved (100 meshes). After charring in a vacuum muffle furnace at 550 °C for 2 h, the surface ash was rinsed off, and the sample was dried after cooling. The material was then modified by treating it with 0.1 mol/L hydrochloric acid for 2 h, followed by rinsing with deionized water until the pH ≈ 7 of the aqueous solution was stable [9–11].

According to the experimental design software, certain masses of nano-titanium and nano-manganese were weighed and added to a fixed mass of SMS-based activated carbon according to the experimental plan. Ultrasonic mixing was carried out, and the antimony solution was adsorbed. After preliminary experiments, the optimal range of conditions was obtained. The experimental design factors and levels for subsequent experiments are shown in the table below.

2.3. Preparation of Nanomaterials

1. The SMS-based activated carbon, nano-titanium, and nano-manganese were added to 20 mL of simulated antimony wastewater solution at a concentration of 12 mg/L. The mass ratios of SMS-based activated carbon to nano-titanium were 4:1, 4:2, 4:3, and 4:4, and the mass ratios of SMS-based activated carbon to nano-manganese were 4:1, 4:2, 4:3, and 4:4. After shaking at room temperature for a certain period, the solution was filtered, and the concentration of antimony was measured using an atomic absorption spectrometer to obtain the experimental results.

Based on (1), the response surface experimental design software Design-Expert was used to determine the optimal mass ratio of nano-titanium (A), nano-manganese (B), and SMS-based activated carbon (C) for removing antimony. The antimony solution was adsorbed according to the experimental scheme. The experimental factors and levels are shown in Table 1.

Table 1. Experimental factor coding and levels.

Influence Factor	Value Level		
	−1	**0**	**1**
SMS-based activated carbon dosage (C)	1:1	3:1	5:1
The dosage of nano-titanium added (A)	0.5	0.75	1
The dosage of nano-manganese added (B)	0.1	0.5	1

2.4. Experimental Methods

The optimal experimental conditions were obtained using single-factor experiments (solid–liquid ratio, pH, adsorption time) and response surface methodology, so as to find the best conditions for removing the heavy metal antimony.

1. A total of 1L of pH = 3, 12 mg/L antimony standard solution was prepared; some 20 mL of standard solution was taken in a brown volumetric flask, and then the nanocomposite material was weighed into the flask. The solid–liquid ratios were 1:1, 2:1, 3:1, 4:1, and 5:1 (mg/mL). Oscillatory adsorption was carried out at room temperature, and the samples were filtered and tested using a Flame Atomic Absorption Spectrometer (FAAS) when the adsorption equilibrium was reached. Three parallel experiments were performed in each group.
2. The above 20 mL of 12 mg/L antimony standard solution was taken in a brown volumetric flask, and the pH of the solution was adjusted with nitric acid and sodium hydroxide (2–10). Then, a certain amount of the nanocomposite was added, and oscillatory adsorption was carried out at room temperature. The samples were filtered and taken after a certain period of time. Three parallel experiments were performed in each group.
3. The above antimony standard solution was taken in a brown volumetric flask; 20 mg of the nanocomposite material was added, and oscillatory adsorption was carried out at room temperature. The adsorption time was set to 15–75 min, and the samples were filtered and taken after a certain period of time. Three parallel experiments were performed in each group.

Design-Expert.10 experimental design software was used in combination with the single-factor test results. The response surface optimization test was designed with pH (A), adsorption time (B), and solid–liquid ratio (C) chosen as the investigation factors and the amount of removal of the heavy metal antimony from nanocomposites taken as the response value. The level values of each factor are shown in the following Table 2.

Table 2. Response surface experimental factor levels.

Level	Adsorption Time (min)	pH	Solid–Liquid Ratios
−1	40	3	7:4
0	45	4	2:1
1	50	5	9:4

3. Results and Discussion

3.1. Optimization of Preparation Conditions of Materials

As shown in Figure 1a, when the mass ratio of SMS-C to Ti gradually decreases, the removal percentage of antimony gradually increases. When the mass ratio reaches 2:1, the removal percentage of antimony remains relatively unchanged. In order to maximize economic benefits, the optimal quality ratio range for SMS-C and Ti is determined to be 2:1–2:1.5. For the ratio of SMS-based activated carbon to nano-manganese, the removal

percentage of antimony initially increases gradually with the mass ratio of SMS-C to Mn from 2:0, reaches its maximum value at 2:0.5, and then begins to decrease. When the mass ratio of Dangdang is lower than 2:0.5, the removal percentage of antimony decreases, which is lower than the adsorption performance of SMS-based activated carbon alone. The possible reason is that excessive nano-manganese blocks some pores of the SMS-based activated carbon, reducing the number of available adsorption sites and thus lowering the antimony removal percentage. Therefore, the optimal range for the mass ratio of SMS-C to Mn is 2:0–2:0.5.

A quadratic regression equation was obtained by using experimental design software to fit the experimental data:

$$Y = 4.89 - 0.054371A - 1.096B + 0.61C + 0.036AB + 0.213AC + 0.1457BC - 0.312A^2 + 1.46B^2 - 0.101C^2 \quad (1)$$

The F value of 66.96 and $p < 0.0001$ indicate that the model is highly significant, with $p = 0.1886$ (>0.05). The R^2 value of 0.9885 indicates that the model is highly significant and reliable. The regression model fits the experimental results well, indicating minimal experimental error and good correlation [16]. Thus, the regression model is reasonable and reliable [17].

In the response surface diagrams b, c, and d, the amount of antimony removal by nano-manganese (B) decreases as the amount of nano-manganese increases. This may be because excessive nano-manganese accumulates on the surface of the carbon, blocking its pores and reducing the adsorption capacity for antimony. Conversely, the removal of antimony increases with the increase in nano-titanium. From the steepness of the surface and contour lines, it is evident that the dosage of nano-titanium (A) has a significant effect on the adsorption of antimony [18].

Based on the model analysis, the optimal mass ratio for antimony removal was determined to be SMS-based activated carbon/Ti/Mn = 1.972:0.993:0.089. To facilitate subsequent experimental operations, this ratio was adjusted to SMS-based activated carbon/Ti/Mn = 2:1:0.1. Since antimony often coexists with lead in nature, due to its occurrence in jamesonite, it is important to consider the removal of lead as well as antimony during the preparation of adsorption materials [19,20]. As shown in Figure 1e, when the dosage ratio is SMS-based activated carbon/Ti/Mn = 2:1:0.5, the material effectively removes both antimony and lead. Therefore, the optimal mass ratio of the composite material was selected as SMS-based activated carbon/Ti/Mn = 2:1:0.5.

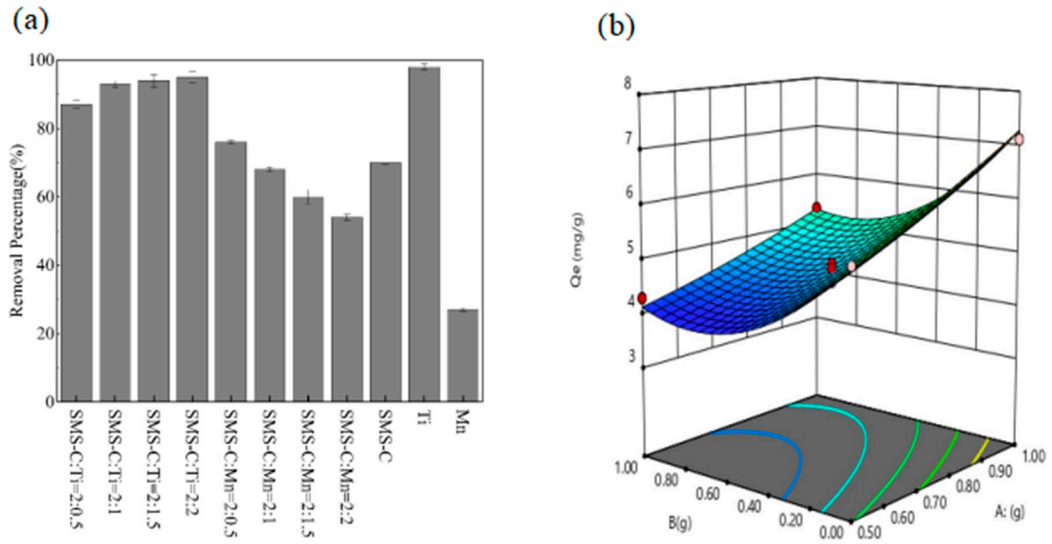


Figure 1. *Cont.*

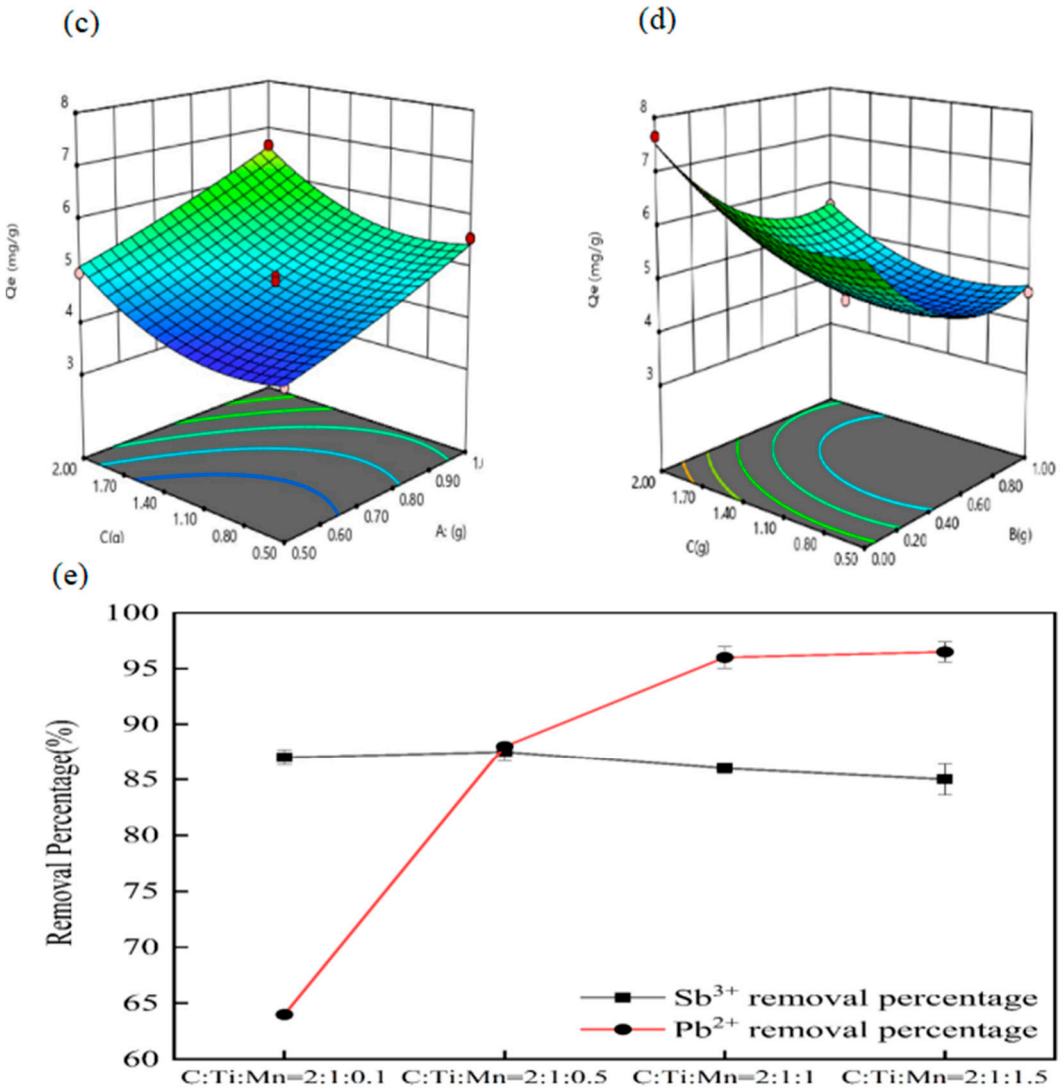


Figure 1. (**a**) The influence of SMS-C: Ti and SMS-C: Mn on the removal of antimony. (**b**) Response surface plots for the removal of antimony by the addition of nano-titanium and nano-manganese. (**c**) Response surface plots for the removal of antimony by the addition of nano-titanium to SMS-based activated carbon. (**d**) Response surface plots for the removal of antimony by the addition of nano-manganese to SMS-based activated carbon. (**e**) The impact of adding nano-manganese on the removal of Sb^{3+} and Pb^{2+}.

3.2. Analysis of Composite Material Characterization Results

In Figure 2a–c, SEM images depict the three preparation stages of the SMS nanocomposites: (a) SMS-based activated carbon, (b) SMS-HCl activated carbon (SMS-based activated carbon modified by hydrochloric acid), and (c) SMS-Ti-Mn nanocomposites. The SEM image of SMS-HCl activated carbon reveals more developed surface porosity, a rougher texture, and an irregular structure. It is evident that the nanomaterials were uniformly loaded onto the surface of SMS-HCl activated carbon without significant agglomeration. Figure 2e shows more pronounced Ti and Mn peaks compared to Figure 2d, which, along with the SEM images, indicate successful loading of nano-titanium and nano-manganese.

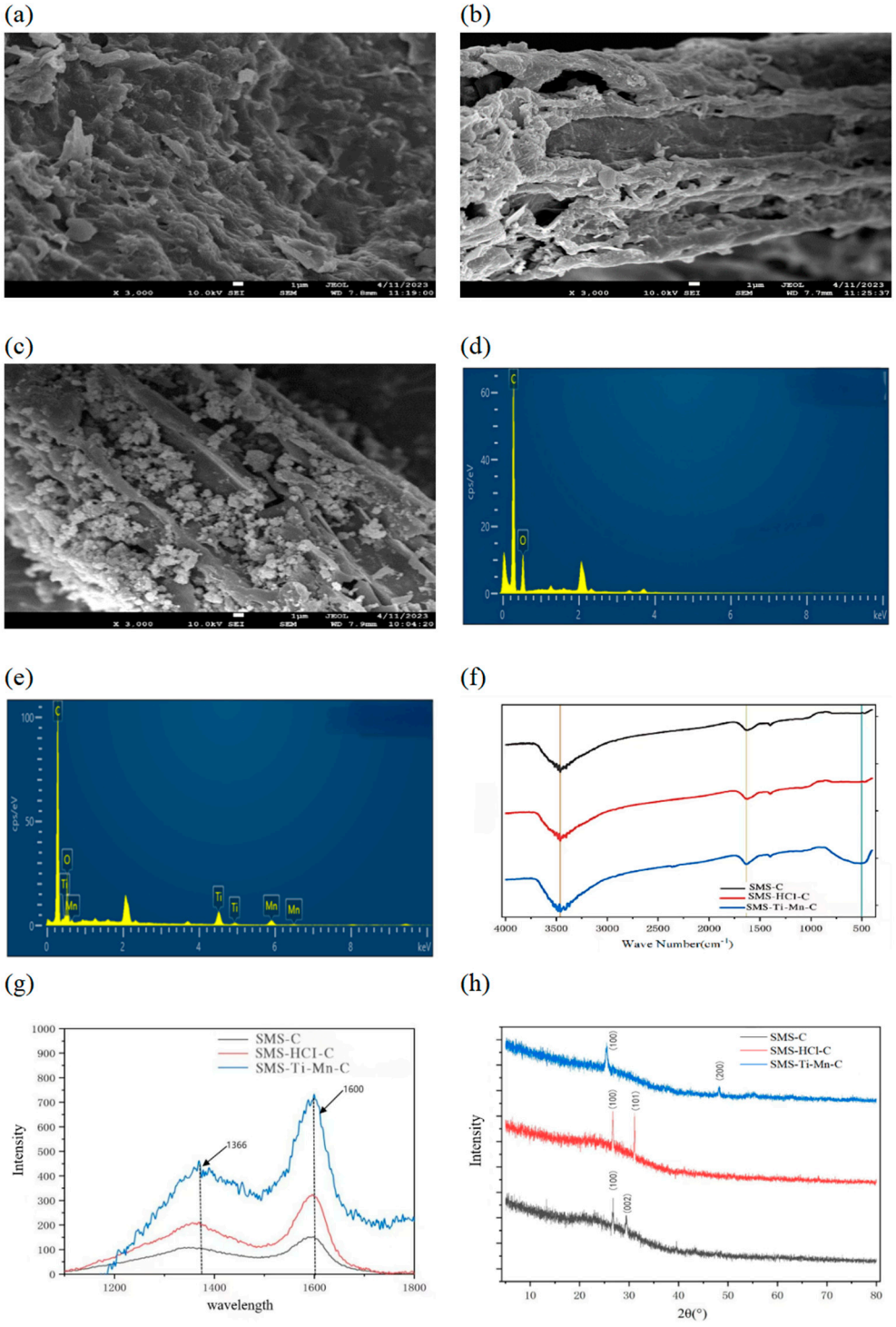


Figure 2. (**a**) Scanning electron microscope image of SMS-based activated carbon. (**b**) Scanning electron microscope image of SMS-HCl activated carbon. (**c**) Scanning electron microscope image of SMS-Ti-Mn nanocomposite. (**d**) Energy spectrum diagram of SMS-HCl activated carbon. (**e**) Energy spectrum diagram of SMS-Ti-Mn nanocomposite. (**f**) Infrared spectrum diagram of activated carbon. (**g**) Raman spectrum diagrams of three materials. (**h**) X-ray diffraction diagrams of three materials.

In Figure 2f, the absorption peaks around 1699 cm^{-1} for all three adsorption materials correspond to the stretching vibration of C=O [21]. Additionally, smaller absorption peaks in the range of 1250–1500 cm^{-1} are observed, corresponding to the stretching vibrations of C-C, C-H, and other skeletal structures, likely due to the presence of lignin and cellulose in SMS-based carbon [22].

All three forms of carbon exhibit distinct absorption peaks around 3431 cm^{-1}, attributed to the stretching vibrations of -OH groups in carboxyl, phenolic, and alcoholic compounds [23]. The absorption peak of the SMS-Ti-Mn nanocomposites near 2346 cm^{-1} is attributed to the stretching vibration of the C=O group in O=C=O. Additionally, an absorption peak at 510 cm^{-1} is observed in the composite material, corresponding to the stretching vibrations of Ti=O and Mn=O groups. The analysis indicates that the functional groups significantly increase following nano-metal loading, with key functional groups including carbonyl, Ti=O, and Mn=O, which promote the adsorption process [24].

In Figure 2g, two prominent peaks are observed at 1366 cm^{-1} and 1600 cm^{-1}. The peak at 1366 cm^{-1} is associated with an amorphous disordered carbon structure, while the peak at 1600 cm^{-1} corresponds to the sp^2 C-C bond vibrations in graphitized carbon, referred to as the D and G bands, respectively. The ID/IG ratios for SMS-based activated carbon (YC), SMS-HCl activated carbon (HCl-C), and SMS-Ti-Mn nanocomposites (FH-C) are 0.656, 0.63, and 0.72, respectively, indicating partial graphitization of all three activated carbon samples [25]. The graphitization degree is the highest for the SMS-Ti-Mn composite and lowest for SMS-HCl activated carbon. This difference is attributed to the increased porosity and pore size of SMS-based activated carbon after activation with HCl, which decreases upon loading with nano-titanium and nano-manganese.

In Figure 2h, the original diffraction peaks of SMS-HCl activated carbon disappear after nano-loading, and new characteristic peaks appear, indicating the adsorption of nanomaterials into the carbon pores, causing pore blockage [26]. At $2\theta = 25.2^\circ$, TiO_2 is in the anatase crystal form, while at $2\theta = 47.9^\circ$, TiO_2 is present in the rutile form, with a relatively low content. At $2\theta = 47.2^\circ$, the diffraction peak corresponds to manganese compounds [27].

3.3. Analysis of Experimental Results

When the solid–liquid ratio of the SMS-Ti-Mn nanocomposites was increased from 1:1 to 5:1, the removal percentage of antimony initially accelerated, achieving rapid growth between 1:1 and 2:1. However, as the solid–liquid ratio increased, adsorption slowed down. Considering economic efficiency, the solid–liquid ratio of 2:1 (mg/mL) was determined to be optimal. When the pH increased from 2 to 10, the antimony removal efficiency first increased and then decreased. Specifically, between pH 2 and 4, the removal percentage gradually increased to a maximum, while between pH 4 and 6, it decreased rapidly. From pH 6 to 10, the decline percentage slowed, with the lowest removal percentage observed at pH 10. Therefore, the optimal removal of antimony was achieved at pH 4. As shown in Figure 3c, during the early stages of the adsorption experiment, the removal percentage increased rapidly, stabilizing as the adsorption time reached 40 min. Between 15 and 40 min, the removal percentage increased steadily. Considering both social and economic benefits, an adsorption time of 40 min was considered the most appropriate for subsequent experiments.

In Figure 3d, the adsorption process of the SMS-Ti-Mn nanocomposites for antimony exhibited an initially rapid phase, which then slowed before reaching dynamic equilibrium at approximately 40 min. This behavior is attributed to the progressive reduction in available adsorption sites over time, leading to a decrease in the adsorption percentage until equilibrium was reached. Both the first-order and second-order R^2 values were greater than 0.98, indicating a good fit for the adsorption kinetics. The correlation coefficient for the first-order kinetic model was higher than that for the second-order model, and the maximum adsorption capacity predicted by the quasi-first-order kinetic model closely matched the experimental results. This suggests that physical adsorption plays a major role in the adsorption process. As shown in the table, both the first-order and second-order

kinetic models had R^2 values greater than 0.98, further confirming their suitability for describing the adsorption kinetics. The first-order kinetic model demonstrated a better correlation, indicating that physical adsorption was the dominant mechanism [28].

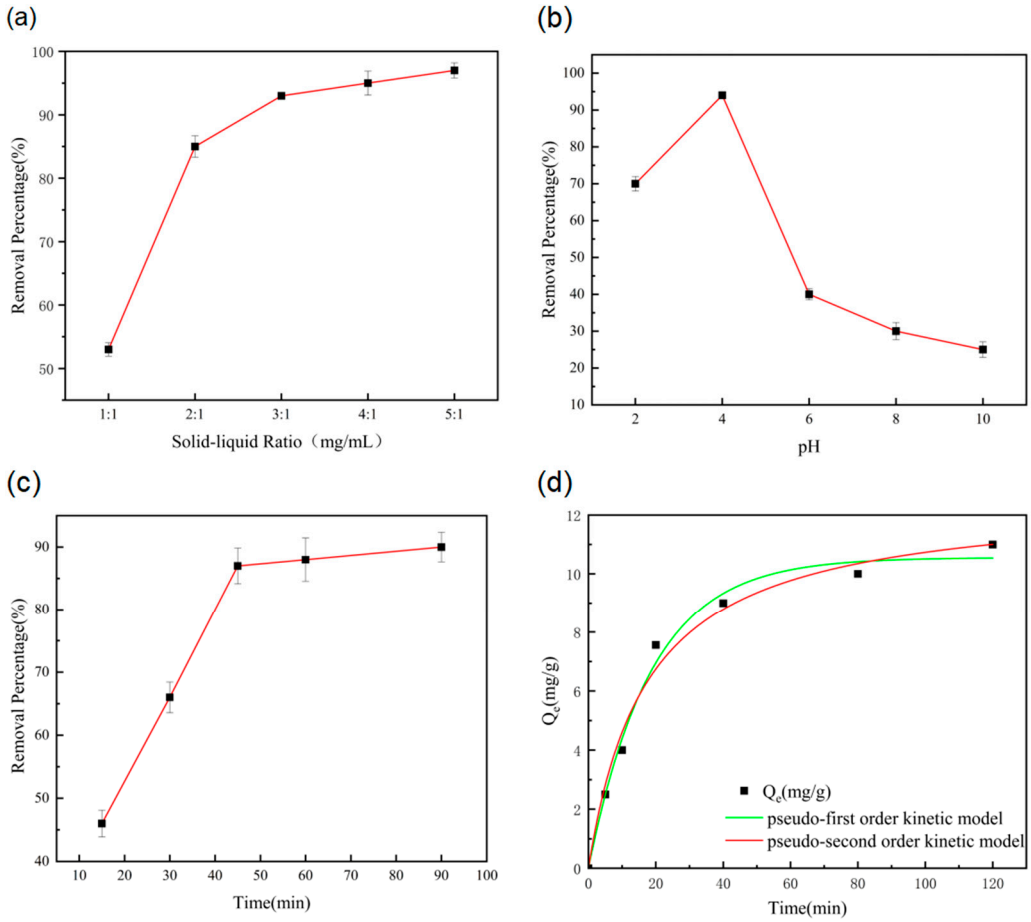


Figure 3. (**a**) Effect of solid–liquid ratio on antimony adsorption capacity of SMS-Ti-Mn nanocomposites. (**b**) Effect of pH on antimony adsorption capacity of SMS-Ti-Mn nanocomposites. (**c**) Effect of adsorption time on antimony adsorption capacity of SMS-Ti-Mn nanocomposites. (**d**) Kinetics curve of antimony adsorption by SMS-Ti-Mn nanocomposites.

Residuals can be used to evaluate the rationality of regression models. As can be seen from Figure 4a, each experimental point is reasonably distributed, mainly on both sides of the straight line. It can be seen from Figure 4b that all 12 groups of values are distributed within the confidence interval, which indicates that when the predicted value of the model is within the range of the internal residual value of ±4.819, the predicted value of the model has high confidence.

Using Design-Expert software, multiple regression analysis was performed on the experimental data. The regression equation for antimony adsorption (Y) was established as follows:

$$Y = 10.296 - 0.81A + 0.1490B + 0.222C - 0.04969AB + 0.1352AC + 0.18299BC - 4.3185A^2 + 0.3534B^2 - 0.3178C^2 \quad (2)$$

The F value of 96.61 and $p < 0.0001$ indicate that the model is highly significant and reliable. The regression model fits the experimental data well, as evidenced by the low experimental error ($p = 0.0844 > 0.05$) and the high correlation ($R^2 = 0.992$). The optimal conditions for antimony removal were found to be a pH of 3.983, an adsorption time of

40.258 min, and a material-to-liquid ratio of 2:1 (mg/mL), with an experimental prediction value of 10.502 mg/g.

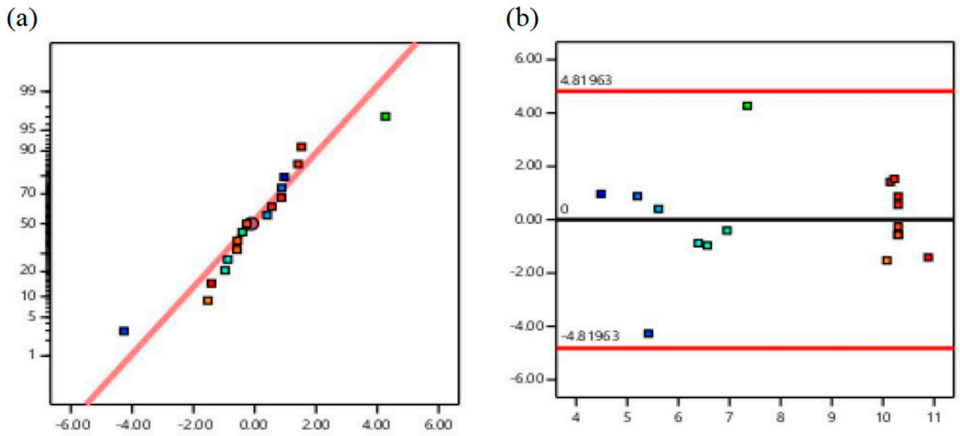


Figure 4. (**a**) Residual normal distribution diagram. (**b**) Relationship diagram between residuals and predicted values.

As shown in Figure 5a, the experimental points are well distributed, primarily on either side of the straight line. In Figure 5b, all 12 groups of values lie within the confidence interval, indicating that when the predicted value falls within the internal residual value range of ±4.819, it has high confidence. The above analysis shows that the regression model has low error, high reliability, and high precision, making it effective for predicting the adsorption of the heavy metal antimony by SMS-Ti-Mn nanocomposites.

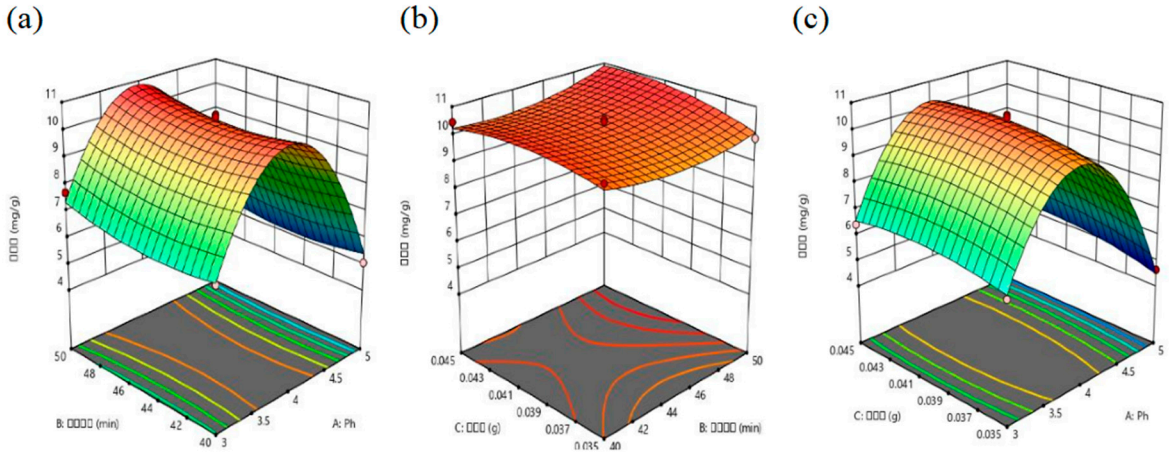


Figure 5. (**a**) Response surface plots of solid–liquid ratio (C) and adsorption time (B). (**b**) Response surface plots of pH (A) and adsorption time (B). (**c**) Response surface plots of solid–liquid ratio (C) and pH (A).

When the solid–liquid ratio is kept constant and only the pH and adsorption time are increased, the adsorption capacity of the SMS-Ti-Mn nanocomposites initially increases and then decreases as the pH increases. In the early stages, the adsorption capacity increases significantly, but after exceeding a certain threshold, it gradually declines. This is because the surface charge of the SMS-Ti-Mn nanocomposites is highly sensitive to changes in the solution pH. When the adsorption time is fixed and only the pH and solid–liquid ratio are increased, the adsorption capacity again shows an initial increase followed by a decrease with increasing pH. When the experimental pH is fixed and both the adsorption time and solid–liquid ratio are increased, the amount of antimony adsorbed by the SMS-Ti-Mn nanocomposites does not change significantly. Based on this analysis, the order of

influence of the different factors on antimony adsorption is as follows: pH > solid–liquid ratio > adsorption time.

3.4. Model Verification

Through analysis using experimental design software, the optimal conditions for the adsorption process of the SMS-Ti-Mn nanocomposites on the heavy metal antimony were determined as follows: adsorption time of 40.258 min, pH of 3.983, and solid–liquid ratio of 2:1 (mg/mL). Under these conditions, the predicted adsorption capacity of the SMS-Ti-Mn nanocomposites for antimony was 10.502 mg/g. Considering practical applications, the experimental conditions were adjusted to an adsorption time of 40 min, a pH of 4, and a solid–liquid ratio of 2:1 (mg/mL) for verification experiments. Three parallel experiments were conducted, and the results showed a maximum adsorption value of 10.392 mg/g, with an average value of 10.34 mg/g. The small error between the predicted and experimental values indicates high consistency, confirming that the model is reliable for predicting antimony adsorption by SMS-Ti-Mn nanocomposites.

4. Conclusions

In this study, SMS-Ti-Mn nanocomposites were successfully synthesized, and their application in removing the heavy metal antimony from water was systematically investigated. By employing single-factor experiments and response surface methodology, the optimal experimental conditions were identified: an adsorption time of 40 min, a pH of 4, and a solid–liquid ratio of 2:1 (mg/mL). Under these conditions, the adsorption capacity of the nanocomposites for antimony reached 10.502 mg/g, which was 5.8 times higher than that of iron coagulants, 11 times higher than that of manganese-modified activated carbon, and 1.7 times higher than that of iron–manganese sludge adsorbents.

Material characterization analysis revealed that the incorporation of nano-metals significantly increased the functional groups present on the activated carbon, particularly carbonyl groups, Ti=O, and Mn=O, which contributed to the enhanced adsorption performance. Adsorption kinetics analysis indicated that physical adsorption played a dominant role in the removal of antimony, with the quasi-first-order kinetic model providing the best fit to the experimental data.

Additionally, the mathematical model established through multiple regression analysis was found to be highly significant, accurately predicting the SMS-Ti-Mn nanocomposites' adsorption capacity for antimony. The experimental results were in strong agreement with the predicted values, demonstrating the high reliability and predictive accuracy of the model.

The findings of this study provide an effective strategy for treating heavy metal-contaminated water and offer important theoretical and practical guidance for the design and optimization of nanocomposites. Future research should further explore the application of these materials in real-world water treatment environments, with particular attention to sustainability and economic viability.

Author Contributions: Conceptualization, M.L.; methodology, F.M.; validation, Y.L., K.L. and Z.F.; formal analysis, S.H.; data curation, W.W.; writing—original draft preparation, Y.L. and W.W.; writing—review and editing, M.L. All authors have read and agreed to the published version of the manuscript.

Funding: We sincerely thank the Scientific Research Foundation of Hainan Tropical Ocean University (No. RHDRC202107), the Major Science and Technology Program of Yazhou Bay Innovation Institute of Hainan Tropical Ocean University (No. 2023CXYZD001), the Hainan Province Graduate Innovation Research Project (No. Qhys2022-325), and the Hainan Tropical Ocean University Graduate Innovation Research Project (No. RHDYC-202414, No. RHDYC-202330) for the financial support.

Data Availability Statement: The data presented in this study are available on request from the corresponding author.

Conflicts of Interest: The authors declare no conflicts of interest.

References

1. Chapa-Martínez, C.; Hinojosa-Reyes, L.; Hernández-Ramírez, A.; Ruiz-Ruiz, E.; Maya-Treviño, L.; Guzmán-Mar, J. An evaluation of the migration of antimony from polyethylene terephthalate (PET) plastic used for bottled drinking water. *Sci. Total Environ.* **2016**, *565*, 511–518. [CrossRef]
2. Zhu, J.; Wu, F.; Deng, Q.; Shao, S.; Mo, C.; Pan, X.; Li, W.; Zhang, R. Environmental characteristics of water body around Tin mine Mountain in Hunan Province. *J. Environ. Sci.* **2009**, *29*, 655–661. [CrossRef]
3. Földi, C.; Sauermann, S.; Dohrmann, R.; Mansfeldt, T. Traffic-related distribution of antimony in roadside soils. *Environ. Pollut.* **2018**, *237*, 704–712. [CrossRef]
4. Li, J.; Duan, H.; Shi, P. Heavy metal contamination of surface soil in electronic waste dismantling area: Site investigation and source apportionment analysis. *Waste Manag. Res.* **2011**, *29*, 727–738. [CrossRef]
5. Abdeldayem, R. A preliminary study of heavy metals pollution risk in water. *Appl. Water Sci.* **2019**, *10*, 1. [CrossRef]
6. Xie, J. Preparation of Manganese Oxide Modified Active Carbon and Its Removal of Thallium. Master's thesis, Hunan University, Changsha, China, 2019. [CrossRef]
7. Iqbal, J.; Shah, N.S.; Sayed, M.; Niazi, N.K.; Imran, M.; Khan, J.A.; Khan, Z.U.H.; Hussien, A.G.S.; Polychronopoulou, K.; Howari, F. Nano-zerovalent manganese/biochar composite for the adsorptive and oxidative removal of Congo-red dye from aqueous solutions. *J. Hazard. Mater.* **2021**, *403*, 123854. [CrossRef] [PubMed]
8. Phenrat, T.; Saleh, N.; Sirk, K.; Tilton, R.D.; Lowry, G.V. Aggregation and sedimentation of aqueous nanoscale zerovalent iron dispersions. *Environ. Sci. Technol.* **2007**, *41*, 284–290. [CrossRef] [PubMed]
9. Li, X.; Huang, J.; Shi, Z.; Xie, Y.; Xu, Z.; Long, J.; Song, G.; Wang, Y.; Zhang, G.; Luo, X.; et al. Reduction and adsorption of uranium(VI) from aqueous solutions using nanoscale zero-valent manganese. *J. Environ. Manag.* **2023**, *342*, 118088. [CrossRef]
10. Liu, Y.-K. Analysis of Photocatalyst and Catalytic Oxidation Mechanism of Nano-Sized Titanium Dioxide Modified by Doped Metal Ions Supported by Activated Carbon. Master's Thesis, Shandong Jianzhu University, Jinan, China, 2018.
11. Zhang, G. Study on the Removal of Antimony (Sb) from Water by Activated Carbon Loaded Titanium Dioxide. Master's Thesis, Kunming University of Science and Technology, Kunming, China, 2017.
12. Ma, J.; Li, F.; Qian, T.; Liu, H.; Liu, W.; Zhao, D. Natural organic matter resistant powder activated charcoal supported titanate nanotubes for adsorption of Pb(II). *Chem. Eng. J.* **2017**, *315*, 191–200. [CrossRef]
13. Duan, G. Study on the Adsorption of Zero Valent Mercury in Coal-Fired Smokeby Modified Manganese Oxides. Master's Thesis, East China University of Science and Technology, Shanghai, China, 2023.
14. Sun, M.; Miao, J.; Tong, X.; Zuo, M.; Song, Z.; Chen, H.; Cheng, G. A new strategy for utilization of gasification ash: Manganese oxides-modified activated carbon for efficient copper citrate removal. *J. Environ. Manag.* **2024**, *365*, 121628. [CrossRef]
15. Shen, Y.; Yue, X.; Wu, T.; Liu, X. Treatment of wastewater with high ammonia nitrogen by manganese dioxide modified activated carbon three-dimensional electrode oxidation. *Mod. Chem. Res.* **2021**, *23*, 168–170.
16. Herath, G.A.D.; Poh, L.S.; Ng, W.J. Statistical optimization of glyphosate adsorption by biochar and activated carbon with response surface methodology. *Chemosphere* **2019**, *227*, 533–540. [CrossRef] [PubMed]
17. Rani, R.; Tasmeem, S.; Malik, A.; Garg, V.K.; Singh, L.; Dhull, S.B. Optimization of Swiss blue dye removal by cotton boll activated carbon: Response surface methodological approach. *Toxin Rev.* **2022**, *41*, 298–314. [CrossRef]
18. Dzigbor, A.; Chimphango, A. Production and optimization of NaCl-activated carbon from mango seed using response surface methodology. *Biomass Convers. Biorefin.* **2019**, *9*, 421–431. [CrossRef]
19. Wang, L. Study on the flotation separation of jamesonite and galena. *Multipurp. Util. Miner. Resour.* **2017**, *2*, 53–57.
20. Nong, Y.P.; Wu, W.; Ye, Y.M. Research on Fe Reaction Behavior in Molten Salt Smelting Process of jamesonite. *China Nonferrous Metall.* **2023**, *52*, 94–104.
21. Jiang, R.J.; Si, Y.X.; Zhang, W.J. Optimization of methylene blue adsorption in water by bacterial residue activated carbon using response surface methodology. *Sci. Technol. Eng.* **2023**, *23*, 7468–7477.
22. Prakash, M.O.; Raghavendra, G.; Ojha, S.; Panchal, M. Characterization of porous activated carbon prepared from arhar stalks by single step chemical activation method. *Mater. Today Proc.* **2021**, *39*, 1476–1481. [CrossRef]
23. Li, X.; Qiu, J.; Hu, Y.; Ren, X.; He, L.; Zhao, N.; Ye, T.; Zhao, X. Characterization and comparison of walnut shells-based activated carbons and their adsorptive properties. *Adsorpt. Sci. Technol.* **2020**, *38*, 450–463. [CrossRef]
24. Ma, W.; Li, H.; Yao, X.; Li, L.; Shih, K. Preparation of hydroPhilic activated carbon through alkaline hydrolysis of ester for effective water-vapor adsorption. *Sep. Sci. Technol.* **2016**, *51*, 193–201. [CrossRef]

25. Gao, G. Thermochemical Modification, Patterning, and Raman Characterization of Graphene. Master's Thesis, Harbin Institute of Technology, Harbin, China, 2014.
26. Irfan, M.; Nawaz, R.; Khan, J.A.; Ullah, H.; Haneef, T.; Legutko, S.; Rahman, S.; Józwik, J.; Alsaiari, M.A.; Khan, M.K.A.; et al. Synthesis and Characterization of Manganese-Modified Black TiO_2 Nanoparticles and Their Performance Evaluation for the Photodegradation of Phenolic Compounds from Wastewater. *Materials* **2021**, *14*, 7422. [CrossRef]
27. Sara, C.A.; Sousa, J.C.; Cardoso, O.C. Monteiro. Improved performance of titanate nanostructures for manganese adsorption and posterior pollutants photocatalytic degradation. *J. Photochem. Photobiol. A Chem.* **2019**, *378*, 9–16. [CrossRef]
28. Bolster, C.H. Kinetics of phosphorous sorption to biochar-amended soils. *Chemosphere* **2023**, *345*, 140523. [CrossRef]

Disclaimer/Publisher's Note: The statements, opinions and data contained in all publications are solely those of the individual author(s) and contributor(s) and not of MDPI and/or the editor(s). MDPI and/or the editor(s) disclaim responsibility for any injury to people or property resulting from any ideas, methods, instructions or products referred to in the content.